

Concepts for Synthetic Aperture Sonar Performance Prediction and Mission Planning

James D. Campbell

Applied Signal Technology, Inc.
Sensor Signal Processing Group *
21311 Hawthorne Blvd., Suite 300
Torrance, CA 90503

Enson Chang

Applied Signal Technology, Inc.
Sensor Signal Processing Group *
21311 Hawthorne Blvd., Suite 300
Torrance, CA 90503

* Formerly Dynamics Technology, Inc.

Abstract – Synthetic aperture sonar (SAS) is an emerging technology capable of providing high resolution seafloor imaging. One remarkable property of SAS is that its azimuthal resolution is theoretically independent of range and wavelength. Consequently SAS is particularly well suited for classifying bottom mines at standoff ranges. SAS processing technology has matured sufficiently in the recent years that it is now being implemented in an entire new generation of platforms, including unmanned underwater vehicles (UUVs). In these applications it is desirable to have an efficient way of estimating SAS performance as a function of environmental and system parameters. Such a capability can serve as a tactical decision aid to optimize performance during a mission. It can also serve as a mission planning or post-mission analysis tool. A series of analytical engineering formulas is given for estimating SAS algorithm performance under various conditions. The formulas are simple in computation yet capable of capturing the most relevant physics. The aggregate of these formulas allows one to quickly estimate the overall system performance. This approach can be extended to provide the basis for a SAS mission planning capability. Concepts for a SAS mission planner are presented.

I. INTRODUCTION

Synthetic Aperture Sonar (SAS) is a technique for processing receive data from a moving hydrophone array to produce high resolution seafloor imagery. During SAS operation, the sonar transmits a pulse at a regular interval as the system moves through the water. The corresponding receive data are synthesized by the SAS processor across multiple consecutive pulses in order to form a long coherent acoustic aperture. The azimuthal (or cross-range) resolution of the resulting imagery is in many cases orders-of-magnitude higher than the resolution of the corresponding real aperture imagery.

One remarkable property of the SAS imagery is that its cross-range resolution is theoretically independent of range and wavelength. This makes SAS an ideal technology for classifying bottom mines at standoff ranges. With rapid maturation of SAS processing technology in recent years, SAS is now being implemented in an entire new generation of

platforms, including unmanned underwater vehicles (UUVs). In these applications it is desirable to have an efficient way of estimating SAS performance as a function of environmental and system parameters. Such a capability can serve as a tactical decision aid to optimize performance during a mission. Performance estimates are also needed to guide mission planning activities and to ensure that mission objectives are accomplished.

Synthetic Aperture Sonar performance is most sensitive to vehicle sway and yaw relative to the slant-range plane. We define sway to be the deviation of the sonar in the slant range direction from an ideal straight-line path, and we define yaw to be the deviation of sonar orientation about slant-range “down” from the orientation of the linear path. The most effective way to counter yaw is to measure it with the navigation hardware. Vehicle sway, on the other hand, is difficult to measure with sufficient accuracy. The redundant phase center (RPC) algorithm, also known as the displaced phase center (DPC) algorithm, is the primary tool used in SAS processing to infer vehicle sway. Since RPC operates on acoustic data, RPC performance, and hence SAS performance, is primarily determined by the ping-to-ping coherence of the received signals. For shallow-water minehunting applications, the two primary factors determining signal coherence are temporal multipath and raw signal-to-noise ratio (SNR).

In the following sections we develop a series of analytical or semi-analytical “engineering formulas” to describe the effect of temporal multipath and raw SNR on SAS performance under various conditions. The formulas include:

1. The effect of multipath and surface wave motion on signal coherence
2. The connection between correlation coefficient and SNR between two redundant time series
3. The sway estimation variance of the RPC algorithm as a function of SNR
4. The effect of RPC estimation errors on image quality

The driving philosophy behind the formulas is that they should be simple in computation and yet capable of capturing the most relevant physics. Their aggregate allows one to quickly estimate the overall system performance.

This work was funded by the Office of Naval Research, contract number N00014-03-M-0208

We will treat the effect of residual phase errors on autofocusing by a simple rule of thumb. The effectiveness of autofocusing algorithms depends strongly on the statistics of the residual phase error. It is difficult to derive a general formula to account for all possible cases of interest. We adopt an empirical rule that autofocusing can achieve ideal response if the residual phase error (after RPC corrections) is less than 3 equivalent range resolution cells. If the residual phase error is larger than this quantity, we assume autofocusing fails and basically does not affect the magnitude of the error.

II. SIGNAL DECORRELATION DUE TO MULTIPATH

This section derives an expression for the correlation coefficient between two redundant time series. If the environment remains static during the time lag between two pings, then the two time series should be identical (except for a possible shift due to platform sway). However, in a multipath environment the surface reflected path(s) will be different between the two pings due to surface motion during the time lag. The result is degraded correlation. The derivation of the correlation coefficient below is based on a point target.

We first consider the simplest case of one direct path and one surface reflected path, as shown in Fig. 2.1. The surface reflected path has a path length of r_1 going from the source to the surface and then to the target. The return leg is assumed to be direct, which has a length of r_0 . The nominal scattering angle of the surface-reflected leg is denoted by θ .

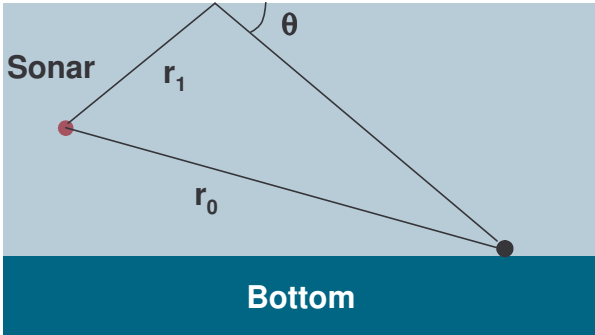


Fig. 2.1. The direct and once-reflected paths to a point target

The total signal for the n^{th} ping is the sum of the two paths and can be written as

$$s_n(t) = u\left(t - \frac{2r_0}{c}\right) \exp\left[i\omega_0\left(t - \frac{2r_0}{c}\right)\right] + Ru\left(t - \frac{r_{1n} + r_0}{c}\right) \exp\left[i\omega_0\left(t - \frac{r_{1n} + r_0}{c}\right)\right] \quad (2.1)$$

where u is the slowly-varying envelope of the narrow-band signal, centered at frequency $f_0 = \omega_0/2\pi$, and R is the reflection coefficient of the surface. The notation r_{1n} makes it clear that it represents the surface-reflected path for the n th ping.

The cross correlation between the two redundant time series is then given by

$$\begin{aligned} \langle s_n(t) s_{n+1}^*(t') \rangle &= u\left(t - \frac{2r_0}{c}\right) u^*\left(t' - \frac{2r_0}{c}\right) \exp[i\omega_0(t - t')] \\ &+ R \left\langle u\left(t - \frac{r_{1n} + r_0}{c}\right) \exp\left[i\omega_0\left(t - \frac{r_{1n} + r_0}{c}\right)\right] \right\rangle \times \\ &\quad u^*\left(t' - \frac{2r_0}{c}\right) \exp\left[-i\omega_0\left(t' - \frac{2r_0}{c}\right)\right] \\ &+ R^* \left\langle u^*\left(t' - \frac{r_{1n+1} + r_0}{c}\right) \exp\left[-i\omega_0\left(t' - \frac{r_{1n+1} + r_0}{c}\right)\right] \right\rangle \times \\ &\quad u\left(t - \frac{2r_0}{c}\right) \exp\left[i\omega_0\left(t - \frac{2r_0}{c}\right)\right] \\ &+ |R|^2 \left\langle u\left(t - \frac{r_{1n} + r_0}{c}\right) u^*\left(t' - \frac{r_{1n+1} + r_0}{c}\right) \right\rangle \times \\ &\quad \exp\left[i\omega_0\left(t - \frac{r_{1n} + r_0}{c}\right)\right] \exp\left[-i\omega_0\left(t' - \frac{r_{1n+1} + r_0}{c}\right)\right] \end{aligned} \quad (2.2)$$

In RPC we seek to maximize the function

$$C(\Delta t) = \langle s_n(t) s_{n+1}^*(t + \Delta t) \rangle \quad (2.3)$$

In the absence of any surface motion, the quantity is maximized by setting $\Delta t = 0$. We want to know how this equal-time correlation degrades with surface motion. Combining (2.2) and (2.3) for $t' = t$, we find

$$\begin{aligned} \int \langle s_n(t) s_{n+1}^*(t) \rangle dt &= \int \left| u\left(t - \frac{2r_0}{c}\right) \right|^2 dt \\ &+ \int R \left\langle u\left(t - \frac{r_{1n} + r_0}{c}\right) \exp\left(-i\frac{\omega_0 r_{1n}}{c}\right) \right\rangle u^*\left(t - \frac{2r_0}{c}\right) \exp\left(i\frac{\omega_0 r_0}{c}\right) dt \\ &+ \int R^* \left\langle u^*\left(t - \frac{r_{1n+1} + r_0}{c}\right) \exp\left(i\frac{\omega_0 r_{1n+1}}{c}\right) \right\rangle u\left(t - \frac{2r_0}{c}\right) \exp\left(-i\frac{\omega_0 r_0}{c}\right) dt \\ &+ \int |R|^2 \left\langle u\left(t - \frac{r_{1n} + r_0}{c}\right) u^*\left(t - \frac{r_{1n+1} + r_0}{c}\right) \exp\left[i\frac{\omega_0}{c}(r_{1n+1} - r_{1n})\right] \right\rangle dt \end{aligned} \quad (2.4)$$

The first term on the right hand side of the equation is due to the direct path. The two middle terms are negligible if r_{1n} and r_{1n+1} are more than a range resolution longer than r_0 since then the two envelope functions in each of these terms do not overlap in time. The last term is due to the surface-reflected path and can decorrelate due to surface wave motion. We will concentrate on this term below.

Now, let the two surface-reflected paths be given by

$$\begin{aligned} r_{1n} &= \bar{r}_1 + 2h_n \sin \theta \\ r_{1n+1} &= \bar{r}_1 + 2h_{n+1} \sin \theta \end{aligned} \quad (2.5)$$

where \bar{r}_1 is the reflected path length in the absence of any surface wave, and h_n is the surface height (due to large scale surface waves) at the nominal reflection point. Then with some simple manipulations the last term in (2.4) becomes

$$\left\langle \int |\tilde{u}(\omega)|^2 \exp \left[2i \frac{\omega}{c} (h_{n+1} - h_n) \sin \theta \right. \right. \\ \left. \left. + 2i \frac{\omega_0}{c} (h_{n+1} - h_n) \sin \theta \right] \frac{d\omega}{2\pi} \right\rangle \quad (2.6)$$

where

$$\tilde{u}(\omega) = \int u(t) \exp(-i\omega t) dt \quad (2.7)$$

Assuming a Gaussian surface height distribution, the ensemble average above can be written as

$$\int |\tilde{u}(\omega)|^2 \exp \left[\frac{2i \sin \theta}{c} (\omega_0 + \omega) (h_{n+1} - h_n) \right] \times \\ p(h_n, h_{n+1}) dh_n dh_{n+1} \frac{d\omega}{2\pi} \quad (2.8)$$

where p is the joint probability distribution for obtaining the two heights at the two ping times, i.e.,

$$p(h, h') = \frac{1}{2\pi\sigma_h^2 \sqrt{1-C_h^2}} \exp \left[-\frac{h^2 - 2C_h h h' + h'^2}{2\sigma_h^2 (1-C_h^2)} \right] \quad (2.9)$$

where σ_h is the rms surface height, and C_h is the normalized surface height correlation function for two different times.

Carrying out the integral in (2.8) and substituting the result back into (2.4), we find

$$\int \langle s_n(t) s_{n+1}^*(t) \rangle dt = \int \left| u \left(t - \frac{2r_0}{c} \right) \right|^2 dt \quad (2.10) \\ + |R|^2 \int |\tilde{u}(\omega)|^2 \exp \left[-4\sigma_h^2 \frac{(\omega_0 + \omega)^2}{c^2} \sin^2 \theta (1-C_h) \right] \frac{d\omega}{2\pi}$$

The integrals can be carried out easily if we assume the pulse envelope to be Gaussian:

$$u(t) = \frac{1}{\sqrt{2\pi}\sigma_t} \exp \left(-\frac{t^2}{2\sigma_t^2} \right) \quad (2.11)$$

The result is

$$\int \langle s_n(t) s_{n+1}^*(t) \rangle dt = \frac{1}{2\pi} \sqrt{\frac{\pi}{\sigma_t^2}} \quad (2.12) \\ + |R|^2 \frac{1}{2\pi} \sqrt{\frac{\pi}{\sigma_t^2 + 4\frac{\sigma_h^2}{c^2} \sin^2 \theta (1-C_h)}} \exp \left(-\frac{\alpha \sigma_t^2 \omega_0^2}{\sigma_t^2 + \alpha} \right)$$

The correlation coefficient is the ratio of this factor to that of the motion-less case

$$\rho = \frac{1 + |R|^2 \frac{\sigma_t}{\sqrt{\sigma_t^2 + \alpha}} \exp \left(-\frac{\alpha \sigma_t^2 \omega_0^2}{\sigma_t^2 + \alpha} \right)}{1 + |R|^2} \quad (2.13)$$

where

$$\alpha \equiv 4 \frac{\sigma_h^2}{c^2} \sin^2 \theta (1-C_h) \quad (2.14)$$

The surface height correlation function C_h is a function of the time separation between the pings and can be computed based on standard surface wave models such as the Pierson-Moskowitz spectrum.

The result above can be extended to account for all lowest order multipaths shown in Fig. 2.2. The correlation coefficient becomes

$$\rho = \left[1 + 4|R|^2 \frac{\sigma_t}{\sqrt{\sigma_t^2 + \alpha}} \exp \left(-\frac{\alpha \sigma_t^2 \omega_0^2}{\sigma_t^2 + \alpha} \right) \right. \\ \left. + |R|^4 \frac{\sigma_t}{\sqrt{\sigma_t^2 + \alpha}} \exp \left(-\frac{2\alpha \sigma_t^2 \omega_0^2}{\sigma_t^2 + 2\alpha} \right) \right] / \left(1 + 4|R|^2 + |R|^4 \right) \quad (2.15)$$

The factor of 4 in front of the middle term (in both the numerator and the denominator) is the result of squaring the sum of the two conjugate paths (path 2 and 3 in Fig. 2.2), which have equal amplitude and phase. The factor of $|R|^4$ represents the contribution of the twice-reflected path (path 4 in Fig. 2.2).

To generalize this result to more paths, this formalism can be applied to the multipath structure identified by ray trace program, such as MineRay. In general, the ray tracer will provide a list of paths with their corresponding amplitude and phase. The general expression for the correlation coefficient is then

$$\rho = \frac{\sum_p |a_p|^2 \frac{\sigma_t}{\sqrt{\sigma_t^2 + K_p}} \exp \left(-\frac{K_p \sigma_t^2 \omega_0^2}{\sigma_t^2 + K_p} \right)}{\sum_p |a_p|^2} \quad (2.16)$$

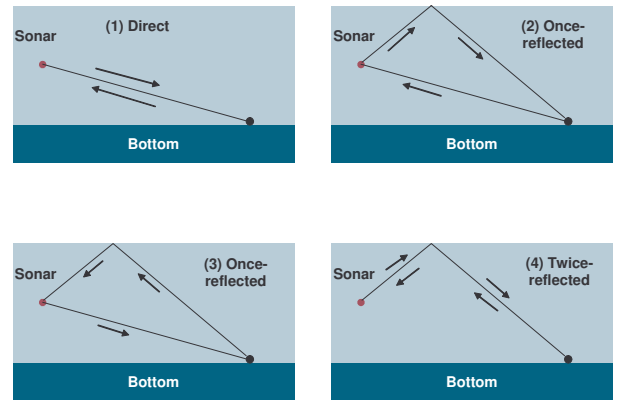


Fig. 2.2. The direct path and three lowest order multipaths to a point target

The sum above is overall all *distinct* paths. Therefore, conjugate paths such as paths 2 and 3 in Fig. 2.2 should be summed into a single path. The coefficients a_p represent the amplitudes of these distinct paths, taking into account

reflection and spreading losses. The factor K_p for each path is the sum of all the α factors, one for each order of surface reflection, of this path. The K_p 's for the first few paths are written out explicitly below:

$$\begin{aligned} \text{Path 1 (Direct path):} & & K_0 &= 0 \\ \text{Path 2+3 (Once-reflected paths):} & & K_1 &= \alpha \\ \text{Path 4 (Twice-reflected path):} & & K_2 &= 2\alpha \end{aligned}$$

Note that α depends on the grazing angle θ . Therefore, in a more complicated situation which may involve several surface reflections at different angles, the coefficient K_p is the sum over all different α 's.

III. CONNECTION BETWEEN CORRELATION AND SNR

Since the RPC sway estimation error depends on the SNR, we need to convert the correlation coefficient calculated above to an equivalent SNR. The connection between the two quantities is simple for additive noise. Let the two time series be denoted by

$$\begin{aligned} s_1(t) &= y(t) + n_1(t) \\ s_2(t) &= y(t) + n_2(t) \end{aligned} \quad (3.1)$$

Assuming that the signal and noise are uncorrelated and that n_1 and n_2 are identically distributed, then we have

$$\left\langle \int s_1(t) s_2^*(t) dt \right\rangle = \left\langle \int |y(t)|^2 dt \right\rangle \quad (3.2)$$

$$\begin{aligned} \left\langle \int s_1(t) s_1^*(t) dt \right\rangle &= \left\langle \int s_2(t) s_2^*(t) dt \right\rangle \\ &= \left\langle \int |y(t)|^2 dt \right\rangle + \left\langle \int |n(t)|^2 dt \right\rangle \end{aligned} \quad (3.3)$$

where

$$\begin{aligned} \left\langle \int |n(t)|^2 dt \right\rangle &= \left\langle \int |n_1(t)|^2 dt \right\rangle \\ &= \left\langle \int |n_2(t)|^2 dt \right\rangle \end{aligned} \quad (3.4)$$

The correlation coefficient between the two time series is then

$$\begin{aligned} \rho &= \frac{\left\langle \int s_1(t) s_2^*(t) dt \right\rangle}{\sqrt{\left\langle \int s_1(t) s_1^*(t) dt \right\rangle} \sqrt{\left\langle \int s_2(t) s_2^*(t) dt \right\rangle}} \\ &= \frac{\left\langle \int |y(t)|^2 dt \right\rangle}{\left\langle \int |y(t)|^2 dt \right\rangle + \left\langle \int |n(t)|^2 dt \right\rangle} \equiv \frac{E}{E+N} \end{aligned} \quad (3.5)$$

Let $SNR = E/N$, then (3.5) can be written as

$$\rho = \frac{SNR}{SNR + 1} \quad (3.6)$$

or alternatively,

$$SNR = \frac{\rho}{1 - \rho} \quad (3.7)$$

IV. ZIV-ZAKAI BOUND OF RPC SWAY ESTIMATE

The sway estimation uncertainty of RPC is directly tied to the SNR of the time series. The SAS literature often cites the Cramer-Rao lower bound (CRLB) of the RPC estimation error. It is well known from time delay estimation literature that the CRLB is overly optimistic at low SNRs. The reason is as follows. The RPC algorithm calculates the complex correlation between the two redundant time series. The resultant correlation function has rapid oscillations enclosed within a slowly varying envelope. (An example is shown in Fig. 4.1 below.) The CRLB corresponds to the estimation error *IF* one knows which peak is the correct peak. At low SNRs, spurious noise can cause one of the neighboring peaks to rise above the correct peak. When this happens, the RPC output can skip an entire cycle, or multiple cycles. This cycle-skipping phenomenon is not accounted for by the CRLB. A more realistic estimate is the Ziv-Zakai Lower Bound (ZZLB).

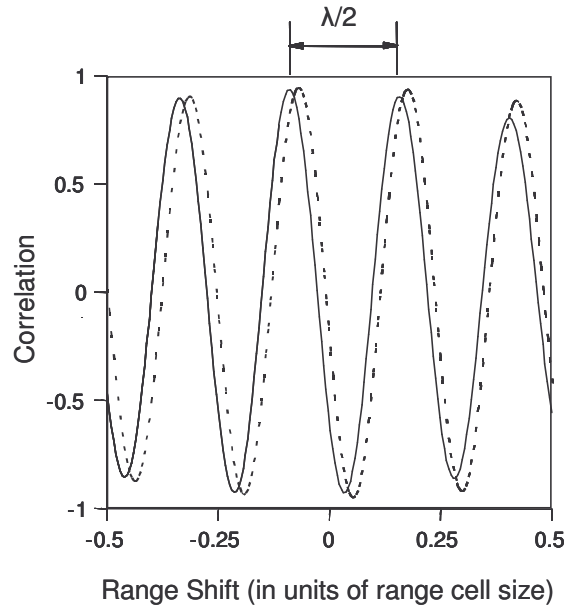


Fig. 4.1. A typical example of the RPC correlation function

The ZZLB for a narrowband signal with Gaussian statistics, as derived by Weiss and Weinstein [1], is given by

$$\langle \varepsilon^2 \rangle \geq \frac{1}{2\beta^2} \left[\frac{1}{2} - \phi(\eta/f_0) \right] \quad (4.1)$$

$$+ \frac{1}{2\eta^2} \exp \left[-9(\eta/f_0)^4 / 40(WT/2\pi) \right]$$

$$\times \left\{ \begin{aligned} & \left[1 + (\eta/f_0)^2 \right] \phi(\eta/f_0) - \left[1 - (\eta D)^2 / 3 \right] \phi(\eta D) \\ & - \left[\eta/f_0 + \frac{4}{3}\eta D \right] \exp \left[-(\eta/f_0)^2 / 2 \right] / \sqrt{2\pi} \\ & - \frac{1}{3}(\eta D - 4/(\eta D)) \exp \left[-(\eta D)^2 / 2 \right] / \sqrt{2\pi} \end{aligned} \right\}$$

where ε is the time-delay estimation error, i.e., the corresponding sway estimation error is $\varepsilon c/2$. In the equation

above, f_0 is the center frequency of the narrow band signal, D is the maximum expected delay, W is the bandwidth of the signal, and T is the duration of the time series. The three functions η , ϕ , and β are defined by

$$\eta^2 = \frac{W^3 T}{48\pi} \Psi \quad (4.2)$$

$$\beta^2 = \frac{WT}{64\pi} (2\pi f_0)^4 \Psi^2 \quad (4.3)$$

$$\phi(y) = \frac{1}{\sqrt{2\pi}} \int_y^\infty \exp(-t^2/2) dt \quad (4.4)$$

and the SNR-like quantity Ψ is defined by

$$\Psi = \frac{SNR^2}{1 + 2SNR} \quad (4.5)$$

V. EFFECT OF RPC ERROR ON THE POINT RESPONSE

In this section we derive an estimate of the effect of RPC estimation errors on the SAS point response based on the phase error variance derived under the ZZLB. It is straightforward to show that the SAS point response in the presence of the RPC phase error is given by the following function

$$C(u) = \int_0^L \exp[iux + i\phi_\varepsilon(x)] dx \quad (5.1)$$

where u is related to the azimuthal position x' (relative to the center of the point response) in the SAS image by

$$x' = \frac{yu\lambda}{4\pi} \quad (5.2)$$

y is the range of the point target, L is the length of the SAS integration aperture, and $\phi_\varepsilon(x)$ is the phase error at azimuthal position x . The ensemble averaged point response is

$$\begin{aligned} \langle |C(u)|^2 \rangle &= \left\langle \sum_{j=1}^N \exp(iux_j + i\phi_j) \times \right. \\ &\quad \left. \sum_{p=1}^N \exp(-iux_p - i\phi_p) \right\rangle \Delta x^2 \end{aligned} \quad (5.3)$$

where we have discretized the integrals and introduced some abbreviations

$$\begin{aligned} N\Delta x &= L \\ x_j &= (j-1)\Delta x \\ \phi_j &= \phi_\varepsilon(x_j) \end{aligned} \quad (5.4)$$

The RPC estimation error accumulates according to

$$\phi_j = \phi_0 + \sum_{l=1}^j \Delta\phi_l \quad (5.5)$$

where ϕ_0 is some initial random phase, and $\Delta\phi_l$ is the random error occurring from applying the RPC algorithm to the l^{th} pair of redundant phase centers. In the derivation below we assume

the $\Delta\phi$'s are identically distributed, zero mean, Gaussian white random variables with a variance given by the ZZLB.

Equation (5.3) can now be written as

$$\begin{aligned} \langle |C(u)|^2 \rangle &= \sum_{j,p=1}^N \exp[iu(x_j - x_p)] \times \\ &\quad \left\langle \exp\left(i \sum_{l=1}^j \Delta\phi_l - i \sum_{m=1}^p \Delta\phi_m\right) \right\rangle \Delta x^2 \\ &= \sum_{j,p=1}^N \exp[iu(x_j - x_p)] \times \\ &\quad \left\langle \exp\left(i \sum_{l=\min(j,p)}^{\max(j,p)} \Delta\phi_l\right) \right\rangle \Delta x^2 \end{aligned} \quad (5.6)$$

Using the fact that the $\Delta\phi$'s are independent Gaussians, the ensemble average in the lower of (5.6) can be written as

$$\begin{aligned} \left\langle \exp\left[i \sum_{l=\min(j,p)}^{\max(j,p)} \Delta\phi_l\right] \right\rangle &= \left[\int_{-\infty}^{\infty} \exp(i\Delta\phi) p(\Delta\phi) d\Delta\phi \right]^{|p-j|} \\ &= \left[\int_{-\infty}^{\infty} \exp(i\Delta\phi) \frac{\exp\left(-\frac{\Delta\phi^2}{2\sigma_\phi^2}\right)}{\sqrt{2\pi}\sigma_\phi} d\Delta\phi \right]^{|p-j|} \end{aligned} \quad (5.7)$$

where σ_ϕ is the rms estimation error from RPC.

The integral in (5.7) is easily carried out to yield

$$\left\langle \exp\left[i \sum_{l=\min(j,p)}^{\max(j,p)} \Delta\phi_l\right] \right\rangle = \exp\left(-\frac{\sigma_\phi^2}{2}|p-j|\right) \quad (5.8)$$

Inserting this back into (5.6) and going back to the integral approximation, we obtain

$$\langle |C(u)|^2 \rangle = \int_0^L \exp\left[iu(x-x') - \frac{\sigma_\phi^2}{2\Delta x}|x-x'|\right] dx dx' \quad (5.9)$$

Carrying out the integrals yields

$$\begin{aligned} \langle |C(u)|^2 \rangle &= \left\{ \frac{\sigma_\phi^2}{\Delta x} \left(u^2 + \frac{\sigma_\phi^4}{4\Delta x^2} \right) L \right. \\ &\quad + \left(-u^2 - iu \frac{\sigma_\phi^2}{\Delta x} + \frac{\sigma_\phi^4}{4\Delta x^2} \right) \exp\left[-\left(iu + \frac{\sigma_\phi^2}{2\Delta x}\right)L\right] \\ &\quad + \left(-u^2 + iu \frac{\sigma_\phi^2}{\Delta x} + \frac{\sigma_\phi^4}{4\Delta x^2} \right) \exp\left[\left(iu - \frac{\sigma_\phi^2}{2\Delta x}\right)L\right] \\ &\quad \left. + 2u^2 - \frac{\sigma_\phi^4}{2\Delta x^2} \right\} / \left(u^2 + \frac{\sigma_\phi^4}{4\Delta x^2} \right)^2 \end{aligned} \quad (5.10)$$

This should be normalized by the peak at $u = 0$ and $\sigma_\phi = 0$, which is L^2 . Furthermore, the variance σ_ϕ^2 should be reduced

by a factor equal to the number of phase centers per ping. The final expression is then

$$\begin{aligned} \langle |C(u)|^2 \rangle &= \left\{ \frac{\sigma_\phi^{12}}{\Delta x} \left(u^2 + \frac{\sigma_\phi^{14}}{4\Delta x^2} \right) L \right. & (5.11) \\ &+ 2 \operatorname{Re} \left[\left[-u^2 - iu \frac{\sigma_\phi^{12}}{\Delta x} + \frac{\sigma_\phi^{14}}{4\Delta x^2} \right] \exp \left[- \left(iu + \frac{\sigma_\phi^{12}}{2\Delta x} \right) L \right] \right] \\ &+ 2u^2 - \frac{\sigma_\phi^{14}}{2\Delta x^2} \left. \right\} / \left[L^2 \left(u^2 + \frac{\sigma_\phi^{14}}{4\Delta x^2} \right)^2 \right] \end{aligned}$$

where

$$\sigma_\phi^{12} \equiv \frac{\sigma_\phi^2}{N_r} \quad (5.12)$$

and N_r is the number of receiver elements in the array, i.e., the number of phase centers per ping.

The peak sidelobe occurs at $u = 3\pi/(2L)$. Since the main lobe's peak level also degrades with nonzero σ_ϕ , the peak sidelobe level is the ratio

$$PSL = \frac{\left\langle \left| C \left(\frac{3\pi}{2L} \right) \right|^2 \right\rangle}{\left\langle |C(0)|^2 \right\rangle} \quad (5.13)$$

VI. NUMERICAL RESULTS

To test the engineering formulas, we exercised them with the following example.

- Isovelocity, range-independent environment
 - Bottom depth = 10 – 50 m
 - Source depth = mid water column
 - Target range = 100 m
 - Frequency = 50 kHz, BW = 10 kHz
 - Ping interval = 0.25 sec
 - Surface reflection coefficient = 0.707
 - Wind speed = 2 – 5 m/sec
 - Depression angle = 0 – 20 deg
 - Vertical aperture = 2 – 6 cm
 - Receiver element width = 10 cm
 - Number of receivers = 16
- Taking into account the 4 lowest order paths

Fig. 6.1 shows the correlation coefficient (2.16) of the aggregate signal, including the four lowest order paths, as a function of wind speed. At the lowest wind speed (2 m/s), the correlation coefficient is approximately unity since there is little randomness to the perfectly reflected signal paths. As the wind speed increases, the surface-reflected paths become less and less correlated, resulting in a loss of coherence. However, since the direct path still carries the dominant amount of energy in this geometry, the correlation coefficient degrades to a constant lower limit.

Additional correlation calculations are shown in the following figures. Fig. 6.2 shows the dependence of correlation coefficient on depression angle. The correlation coefficient increases with depression angle because the surface-reflected paths become less important as the sonar points away from the surface. Fig. 6.4 shows that correlation coefficient improves as the vertical aperture of the sonar increases, which has the effect of decreasing the intensity of the surface-reflected paths.

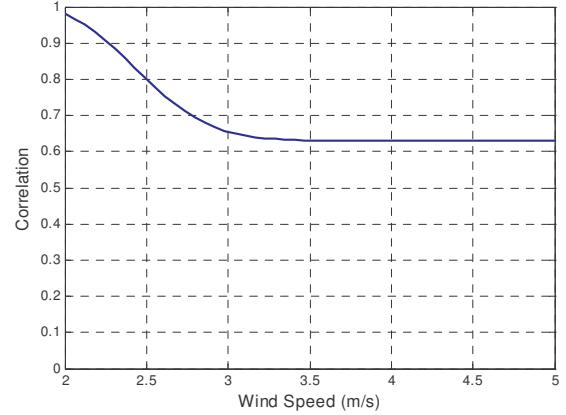


Fig. 6.1. Dependence of the correlation coefficient on wind speed

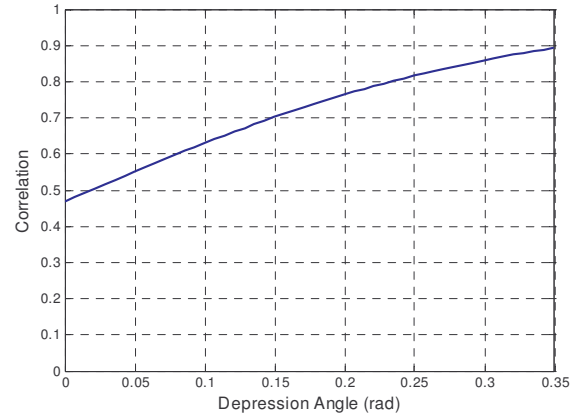


Fig. 6.2. Dependence of the correlation coefficient on depression angle

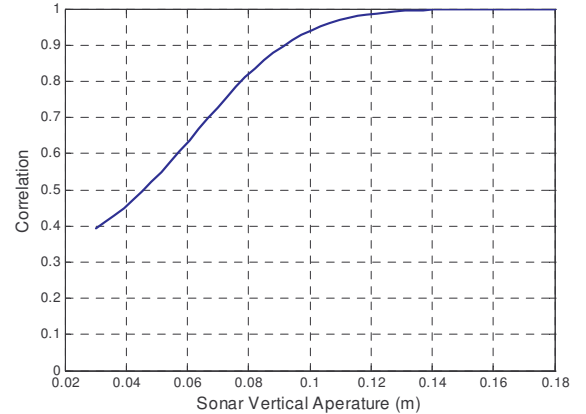


Fig. 6.3. Dependence of the correlation coefficient on sonar vertical aperture

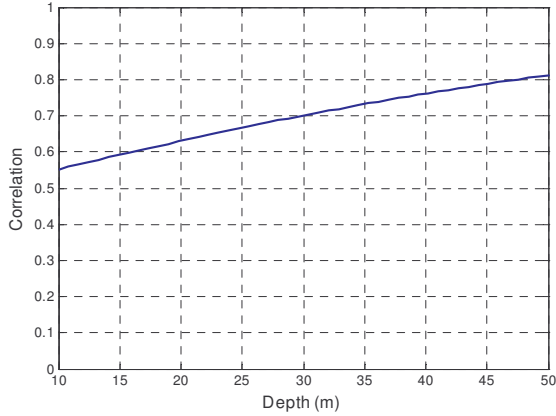


Fig. 6.5: Dependence of the correlation coefficient on depth

Finally, Fig. 6.5 shows increasing correlation as the sonar moves away from the surface, i.e., increasing depth.

Fig. 6.6 is a plot of the SAS point response (5.11) for a wind speed of 2 m/s and a series of different sonar depression angles, ranging from 0 to 20 degrees. At a zero degree depression angle, there is sufficient surface interaction to cause RPC decorrelation, which in turn leads to degradation of the SAS point response. The flattest curve shown in Fig. 6.3 corresponds to this depression angle, indicative of substantial image smearing. As the depression angle is increased, the surface-reflected paths contribute less and less to the overall signal energy. The RPC correlation increases, and the resultant point response becomes sharper. By the time the depression angle is increased to 20 degrees, the SAS point response is essentially ideal.

Fig. 6.7 is a two-dimensional plot showing the dependence of shadow contrast on depression angle and wind speed. This represents the kind of result that these engineering formulas can produce quickly and efficiently to aid the sonar operator in making tactical decisions.

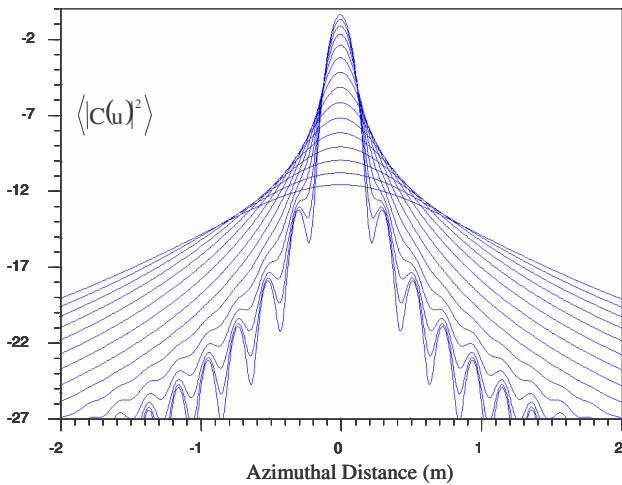


Fig. 6.6. The SAS point response at a wind speed of 2 m/s and for sonar depression angles ranging from 0 to 20 degrees

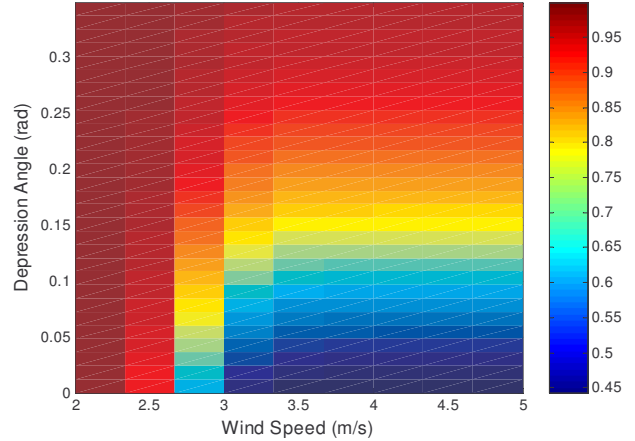


Fig. 6.7. Shadow contrast as a function of depression angle and wind speed

VI. MISSION PLANNER CONCEPTS

As the current generation of SAS-equipped MCM UUVs matures, a corresponding set of MCM SAS Mission Planning (SAS-MP) tools will be needed. Missions will require careful route planning to ensure optimal SAS performance in the strongly varying littoral environment. Furthermore, the vehicle path will need to be specified such that attitude rates do not exceed the performance envelope of the SAS image formation algorithms. Tools will also be needed to optimize search routes and to evaluate mission effectiveness. The engineering formulas developed in the previous sections provide the basis for building a SAS-MP.

The SAS Mission Planner is envisioned to interface primarily with MEDAL, the Navy's single designated Mine Warfare decision support system. The MEDAL toolkit would provide the environmental and mine-threat databases needed to compute SAS performance. SAS-MP, in turn, would provide MEDAL with the required tactical capabilities to create, evaluate, optimize, and transmit MCM plans for SAS-equipped UUVs. SAS-MP mission evaluation capabilities could also interface with the Naval Mine Warfare Simulation (NMWS) while simulating specific missions and evaluating alternative courses of action.

Other existing or developmental products related to a SAS Mission Planner include the following:

1. MCM Expert is the NATO Mine Warfare tool. Synthetic aperture sonar could potentially be added as a sensor in MCM Expert.
2. The Joint Unmanned System Common Control (JUSC2) program is also related to SAS Mission Planning. Although JUSC2 goals are much broader than the scope of a SAS-MP, there is overlap in the area of vehicle control. Additionally, the first phase of JUSC2 will be built on Littoral Combat Ship and Remote Minehunting System, both of which are potential candidates for a SAS-equipped UUVs or USVs.

3. The ARL:UT High Frequency Sonar TDA (STDA) provides capability to optimize sonar lineup (depression/elevation angle, vertical beamwidth, ownship depth recommendation) and to predict detection performance. The engineering formulas that we have developed in the previous sections provide the means to optimize the sonar lineup for a SAS. The predicted SAS point response function could be linked to a detection model to compute detection performance and to provide a capability similar to the STDA.
4. The Autonomous Littoral Warfare Systems Evaluator (ALWSE) toolkit of NSWC Panama City, while not a mission planner, provides the capability to lay out simulated routes and to predict detection performance as a function of position along the route. This capability of predicting performance along a path will be fundamental to SAS mission planning and evaluation tools.

A basic element of a SAS Mission Planner would be a "path engine" for predicting performance at each point along a commanded path. The engineering formulas derived in the previous sections provide the basis for making these calculations along an ideal straight-line path. These formulas can be further modified to include the effects of deviation from the straight line. Deviation includes translational (most importantly, sway and heave) and rotational (importantly, yaw and pitch) motion and can also include crabbing in the presence of tides or ocean currents. Additionally, the effects of navigation system error can be incorporated. The path engine could then compute expected image quality at each point in a surveyed region, including the following image metrics:

1. Resolution
2. Integrated sidelobe ratio
3. Peak sidelobe ratio
4. Pixel geo-location

Ideally, with no phase error present, these metrics would be constant with respect to range. However, in practice we can expect some range dependence. The fourth metric, pixel geo-location, is the expected accuracy to which pixels can be located in a terrestrial reference frame, such as the WGS-84. This is important for re-acquiring objects of interest.

With the path engine in place, a detection/classification model could then translate the predicted image quality metrics and the SNR levels into probability of detection and classification of particular threats. A resolution-dependent detection/classification model could be used to compute these probabilities at each point within a given search area, thus providing a mission performance prediction capability. The probability of detection at each point could be plotted as an overlay on a map of the survey region. Similar overlays could be plotted for each of the image metrics to provide a capability for more detailed analysis. Statistics, such as the max, min, and median of the probability of detection/classification, could be used to evaluate overall mission effectiveness.

The mission planning approach described up to now assumes an operator-entered route. However, it is also

desirable to be able to optimize a search route within certain constraints with respect to a particular performance metric, such as the total search time. Route optimization is admittedly a difficult problem due to the almost infinite number of possible routes and the high computational cost of evaluating each one. One approach to overcoming this problem is to implement search policies. For horizontal position, these might include the following policies:

1. Pushbroom- or lawnmower-pattern
2. Contour-following

Vertical position would be subject to sonar lineup optimization and the motion constraints of the SAS. Heuristics would need to be developed for each policy in order to generate a reasonably small number of candidate routes, each with a high likelihood for optimality. Each candidate route could then be evaluated, and the optimal one selected, within an operationally acceptable amount of computational time. As part of the route optimization process, the expected vehicle dynamics should not be allowed to exceed the motion constraints allowable for SAS image processing.

The SAS-MP would also include an Advanced Users Mode with the capability to generate analysis plots, such as those presented the numerical example of Section 6. The idea in fig. 6.7 could be extended to include any image metric (resolution, ISLR, or PSLR) as a function of any two environmental or system parameters (wind speed, depression / elevation angle, synthetic aperture length, etc). In addition, standard capabilities such as SNR plots and ray trace diagrams would be included.

VII. CONCLUSIONS

The statistical models and the engineering formulas derived in this paper provide the technical basis for building a SAS mission planning capability. These formulas quantify the effects of temporal multipath interference on SAS image quality. The effects of motion and navigation system error will need to be added to these formulas to complete the SAS point response modeling. The resulting image metrics can be linked to probability of detection of a particular target using standard MCM models. With probability of detection calculated at each point in the search area, mission effectiveness can be predicted. A cost function can then be constructed to allow route optimization. Due to the complexity of the optimization problem, empirical heuristics will need to be developed in order to limit the number of candidate routes to an acceptable size. Vehicle motion should be constrained within the performance envelope of the image formation algorithms. Finally, a suite of analysis tools should be included for training and diagnostic purposes. A SAS mission planner built on these concepts will provide an efficient means of utilizing SAS payloads to support undersea missions in a variety of environmental conditions.

REFERENCE

- [1] A.J. Weiss and E. Weinstein, "Fundamental Limitations in Passive Time Delay Estimation – Part I: Narrow-Band Systems," *IEEE Transactions on Acoustics, Speech, and Signal Processing*, vol. ASSP-31, no. 2, pp. 472-486, 1983.